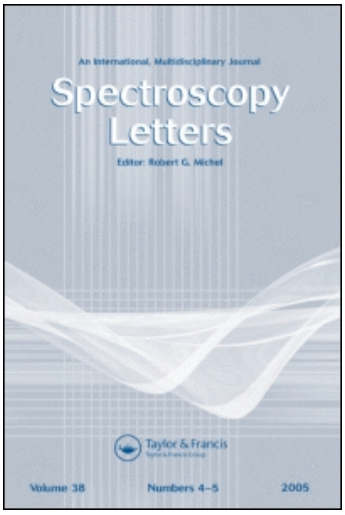

Spectroscopy Letters
Publication details, including instructions for authors and subscription information:
http://www.informaworld.com/smpp/title~content=t713597299

Energy Shift of the $4f^{13}6s^{1}$ Excited States of Yb^{2+} from Gas Phase to the $CsCaBr_3$ Solid

Goar Sánchez-Sanz[a]; Luis Seijo[ab]; Zoila Barandiarán[ab]
[a] Departamento de Qumica, Universidad Autónoma de Madrid, Madrid, Spain [b] Instituto Universitario de Ciencia de Materiales Nicolás Cabrera, Universidad Autónoma de Madrid, Madrid, Spain

Online publication date: 30 July 2010

To cite this Article Sánchez-Sanz, Goar , Seijo, Luis and Barandiarán, Zoila(2010) 'Energy Shift of the $4f^{13}6s^{1}$ Excited States of Yb^{2+} from Gas Phase to the $CsCaBr_3$ Solid', Spectroscopy Letters, 43: 5, 393 — 399
To link to this Article: DOI: 10.1080/00387010.2010.487006
URL: http://dx.doi.org/10.1080/00387010.2010.487006

Spectroscopy Letters, 43:393–399, 2010

ISSN: 0038-7010 print/1532-2289 online
DOI: 10.1080/00387010.2010.487006

Taylor & Francis
Taylor & Francis Group

Energy Shift of the $4f^{13}6s^1$ Excited States of Yb^{2+} from Gas Phase to the $CsCaBr_3$ Solid

Goar Sánchez-Sanz[1], Luis Seijo[1,2], and Zoila Barandiarán[1,2]

[1]Departamento de Qumica, Universidad Autónoma de Madrid, Madrid, Spain
[2]Instituto Universitario de Ciencia de Materiales Nicolás Cabrera, Universidad Autónoma de Madrid, Madrid, Spain

ABSTRACT *Ab initio* calculations on Yb^{2+}-doped $CsCaBr_3$ show a large increase ($20000\,cm^{-1}$) of the $4f^{14} \rightarrow 4f^{13}6s^1$ transitions from gas phase to $CsCaBr_3$, due to large embedding effects originated beyond the first bromide coordination shell. The $4f^{13}6s^1$ states of $(YbBr_6)^{4-}$ *in vacuo* undergo a sudden energy and electron density change at short Br-Yb distances resulting in the formation of an Yb-trapped exciton, which evolves to full ionization, making Yb(II) unstable in hexabromide coordination in gas phase. Embedding in $CsCaBr_3$ localizes the 6*s* electron inside the Br_6 cage, which increases the 6s-Br_6 repulsion and increases the energy of the $4f^{13}6s^1$ states.

KEYWORDS

INTRODUCTION

The emission spectrum of doubly ionized Ytterbium in gas phase was measured by Bryant already in the early 1960s.[1] All 41 energy levels, 28 odd and 13 even, belonging to the $4f^{14}$, $4f^{13}$ $5d^1$, $4f^{13}$ $6s^1$, $4f^{13}$ $6p^1$, and $4f^{13}$ $7s^1$ configurations were experimentally determined and assigned to the appropriate quantum numbers. The second and third excited energy levels, lying at 34656.13 and 34990.66 cm^{-1}, were found to be the $J=4$ and 3 levels of the $4\,f^{13}$ $[7/2(^2F)]6s^1$ $[1/2(^2S)]$ configuration [$4f^{13}$ $(7/2)6s^1$, from now on]; the other two $4f^{13}$ $6s^1$ levels (the 13th and 14th in the emission spectrum), were found some $10300\,cm^{-1}$ above (at 44853.59 and 45207.64 cm^{-1}), and were assigned to the $J=2$ and 3 levels of the $4f^{13}$ $[5/2(^2F)]6s^1$ $[1/2(^2S)]$ configuration [$4f^{13}$ $(5/2)6s^1$, from now on].

A number of experimental reports on the spectroscopy of Yb^{2+}-doped crystals have appeared since the pioneering work of McClure and collaborators[2,3] (see Rubio[4] for a review; for an overview on recent works see Pan et al.[5]), however, the $4f^{13}$ $6s^1$ states have not received much attention, in general, in spite of the fact that they lie comparatively so low in the free ion. In particular, simple and useful models like that of Judd and Morrison[6,7,8] to describe the energy shifts of the $4f^{N-1}$ $5d^1$ states from gas phase to the solid are lacking for the $4f^{N-1}$ $6s^1$ states. The only exception to this we are aware of is found in Ref. 5, where two crystal levels of Yb^{2+} doped in $SrCl_2$, lying at 35028 and 45794 cm^{-1}, were assigned to the $4\,f^{13}$ $6s^1$ configuration, assuming that very small energy shifts and splittings should be expected from the free ion to the host crystal.

Received 18 June 2009; accepted 10 July 2009.

Address correspondence to Zoila Barandiarán, Instituto Universitario de Ciencia de Materiales Nicolás Cabrera, Universidad Autónoma de Madrid, Madrid 28049, Spain. E-mail: zoila.barandiaran@uam.es

On the other hand, *ab initio* quantum chemical calculations have shown that the $4f^{13}$ $6s^1$ states are very strongly destabilized when Yb^{2+} is doped in $CsCaBr_3$ crystals.[9] Whereas they are found at comparable energies, as described above in the free ion calculations, as we show here, which means that the lowest $4f^{13}$ (7/2)$6s^1$ $J=4$, 3 levels are the second and third excited levels in the calculated spectrum, they appear above 54000 cm^{-1} in the crystal, higher in energy than the $4f^{13}$ (7/2)$5d(t_{2g})^1$, $4f^{13}$ (5/2)5 $d(t_{2g})^1$, and $4f^{13}$ (7/2)$5d(eg)^1$ manifolds, and overlapping the $4f^{13}$ (5/2)$5d(e_g)^1$ manifold.[9] Neither dynamic electron correlation nor spin-orbit effects are responsible for the large, positive energy shift, given that their effects are comparable in gas phase and in the $CsCaBr_3$ solid. Therefore, basic bonding interactions (excluding electron correlation) with the bromine ligands and with the rest of the embedding host determine the evolution of the 6*s* electron density and energy from gas phase to the solid. The analysis of these interactions is the subject of this paper. The ultimate goal is to build a simple model that shows the factors that determine the energy shifts of the $4f^{13}$ $6s^1$ states from gas phase to the solids. This matter is related to the ability of the diffuse states of *f*-element ions to behave, alternatively, as localized states or as impurity trapped excitons in ionic solids.

DETAILS OF THE CALCULATIONS

Given the open-shell nature of the electronic states of Yb^{2+}, the wave functions and energies of the ground and excited states of the free ion and the $(YbBr_6)^{4-}$ and $(YbBr_6)^{3-}$ octahedral clusters *in vacuo* are calculated using a multiconfigurational mean-field approximation method (the complete active space self-consistent-field method, CASSCF[10]; see details below). Both the coefficients of the configurational expansion and the coefficients of the basis set used to expand the molecular orbitals are simultaneously and variationally optimized in the CASSCF calculations. At this level of theory, static correlation and scalar relativistic effects (mass-velocity and Darwin) are included, but dynamic electron correlation and spin-orbit coupling is excluded. The CASSCF wave functions are suitable references for ulterior second order multiconfigurational perturbation method calculations when the goal is to retrieve the dynamic electron correlation corrections which would be attained at the full configuration interaction (CI) level. This type of correlated calculations have been done here for the free ion and the method chosen is the so called multi-state complete active space second order perturbation method, MS-CASPT2.[11–14] This level of theory also includes static relativistic effects. The effects of spin-orbit coupling are added through double-group spin-orbit configuration interaction (SO-CI) calculations. The configurational space is small (see below) but the electron correlation retrieved at the MS-CASPT2 level is transferred to this space by the so-called spin-free-state-shifting operator, which ensures that the spectrum of the small CI space coincides with the MS-CASPT2 spectrum in the absence of spin-orbit terms.

All the methods used here have been described elsewhere; more details can be found in Ref. 9. The configurational space of the CASSCF calculations is that resulting from distributing the 14 open-shell electrons in the 13 active molecular orbitals with main character Yb 4*f*, 5*d*, 6*s*. Spin ($S=0$, 1) and spatial symmetry (O_b, but D_{2b} is actually used in the calculations) are the only restrictions imposed and the expansions include some 10^5 configurations among which all states of the $4f^{13}$ $5d^1$ and $4f^{13}$ $6s^1$ configurations appear. The CAS has been reduced to the 4*f* dominant orbitals for the calculation of the ground states.

Relativistic core *ab initio* model potentials (AIMP) have been used to represent the [Kr] core of Yb[15] and the [Ar, 3*d*] core of Br;[16] the corresponding valence basis sets have been used contracted as Yb [6*s* 5*p* 6*d* 4*f* 1*g*] and Br [3*s* 5*p* 2*d*]. Basis functions have also been added outside the cluster in some of the cluster *in vacuo* calculations in order to allow for delocalization of the wave functions, as specified below in our discussion of energy shift analysis. Dynamic electron correlation has been taken into account only in the free ion by multi-state second-order perturbation theory calculations (MS-CASPT2);[11–14] the 32 valence electrons of Yb were correlated. The program MOLCAS has been used for these calculations.[17] Spin-orbit coupling has been included in the free ion calculations using the full Wood-Boring AIMP Hamiltonian;[18,19] the spin-orbit coupling operator has been scaled by a factor of 0.9, as proposed in Barandiaran and Seijo[20]; double-group spin-orbit

configuration-interaction (SO-CI) calculations were done using the spin-free-state-shifting (sfss) operator[21] to transport the dynamic electron correlation effects retrieved at the MS-CASPT2 level. The $4f^{13}$ $5d^1$ and $4f^{13}$ $6s^1$ multireference plus all single excitations from the $4f$, $5d$, and $6s$ molecular orbitals to the virtual orbitals defined the SO-CI space. The calculations have been done using the EPCISO program.[22] All AIMP data and valence basis sets can be found in Reference 23.

RESULTS AND DISCUSSION

Energy Shifts of the $4f^{13}$ $6s^1$ Excited States of Yb^{2+} from Gas Phase to the $CsCaBr_3$ Solid

The calculated $4f^{14} \rightarrow 4f^{13}$ $6s^1$ transition energies of Yb^{2+} in gas phase are shown in Table 1. The results of three different calculations of increasing accuracy are presented. All results include dynamic correlation of the 32 valence electrons, except the CASSCF ones. Spin-orbit coupling is included only in the SO-CI calculations.

The comparison of the CASSCF and MS-CASPT2 results show that dynamic electron correlation increases the transition energies significantly (*ca.* 32000 cm^{-1}) due to the fact that the $4f$-$6s$ electron pairs of the excited states are further apart than the replaced, tight $4f$-$4f$ electron pairs of the ground state, and, hence, the stabilization of electron correlation corrections is much larger for the latter. Spin-orbit coupling results in four levels corresponding to the coupling of the $4f^{13}$ $J=7/2$ and $5/2$ sub-shell with the $6s$ $J=1/2$ electron; their energies deviate from the experimental values by some 2300 cm^{-1} (Table 1). The main effect of spin-orbit is the energy gap between the $4f^{13}$ $(7/2)6s^1$ and $4f^{13}$ $(5/2)6s^1$ states, which is about 10400 cm^{-1}, in agreement with experiment (Table 1).

The large increase provoked by dynamic correlation and the splitting due to spin-orbit coupling we have just mentioned (32000 cm^{-1} and 10400 cm^{-1}, respectively) are very similar to those found in the calculation of the $4f^{14} \rightarrow 4f^{13}6s^1$ transition energies in the $CsCaBr_3$ host[9] (26300 cm^{-1} and 10500 cm^{-1}, respectively). However, the $4f^{13}$ $6s^1$ crystal levels appear much higher in energy. The $4f^{13}$ $(7/2)6s^1$ crystal states are found between 54000 and 59000 cm^{-1}, overlapping and interacting with the $4f^{13}$ $(5/2)5d(e_g)^1$ manifold and the $4f^{13}$ $(5/2)6s^1$ crystal states lie between 66900 and 67500 cm^{-1}.

Therefore, it is possible to conclude that (i) the $4f^{13}$ $6s^1$ states of Yb^{2+} are strongly destabilized from gas phase to the $CsCaBr_3$ crystal by about 20000 cm^{-1}, (ii) dynamic electron correlation and spin-orbit coupling are not responsible for the large and positive energy shifts.

In effect, the strong destabilization of the $4f^{13}$ $6s^1$ states can already be observed comparing the free ion and the embedded cluster CASSCF results, as we show below. Therefore, the interactions leading to the transition energy shifts are included at this level of theory, which can be used for their analysis.

TABLE 1 Transition Energies from the Ground State, $4f^{14}$ ^1S_g $J=0$, to the $4f^{13}$ $6s^1$ Excited States of Yb^{2+} in Gas Phase Calculated without and with Spin-Orbit Coupling

		CASSCF		MS-CASPT2	
Without spin-orbit coupling					
$4f^{13}$ $6s^1$	^3F_u	8600		41200	
	^1F_u	9300		42100	
	J	SO-CI		Experiment [Ref. 1]	
With spin-orbit coupling					
$4f^{13}$ $(7/2)6s^1$	4	36800	(100% ^3F_u)	34656.13	(100% ^3F_u)
	3	37300	(53% ^1F_u)	34990.66	(54% ^1F_u)
$4f^{13}(5/2)6s^1$	2	47155	(100% ^3F_u)	44853.59	(100% ^3F_u)
	3	47619	(51% ^3F_u)	45207.64	(54% ^3F_u)

All but the CASSCF results include dynamic correlation of the 32 valence electrons. See text for details. All numbers in cm^{-1}.

Analysis of the Energy Shifts

As we have commented, whereas the $4f^{13}$ $6s^1$ ^3F_u and ^1F_u states appear at about 8600 and 9300 cm^{-1} (Table 1) and are the second and third excited states of the free ion, the corresponding $4f^{13}$ $6s^1$ T_{1u}, T_{2u}, and A_{2u} states with spin multiplicities $2S+1=3$ and 1 are obtained from 34800 to 35900 cm^{-1}, above all the $4f^{13}$ $5d(t_{2g})^1$ and $4f^{13}$ $5d(e_g)^1$ states of the $CsCaBr_3$: Yb^{2+} crystal,[9] when the calculations are done at the CASSCF level.

Consistent with the embedded cluster model used by Sanchez-Senz et al.[9] it is reasonable to follow the evolution of the CASSCF energy and electronic density of the excited states from gas phase to the host crystal comparing the results of: (a) the free

ion, (b) the $(YbBr_6)^{4-}$ cluster *in vacuo*, and (c) the $(YbBr_6)^{4-}$ cluster embedded in the $CsCaBr_3$ host. In this way, the effects of the Br ligands and the effects of the embedding host can be observed separately.

The CASSCF results of the free ion have been commented above (Table 1). We present the calculated CASSCF energy curves for the $4f^{14}$–$^1A_{1g}$ ground state and the (representative) $4f^{13}\ 6s^1$–$^3A_{2u}$ excited state of the $(YbBr_6)^{4-}$ cluster *in vacuo* on the left, upper graph of Fig. 1. The CASSCF energy curves of the same states of the $(YbBr_6)^{4-}$ cluster embedded in $CsCaBr_3$[9] are plotted on the right of Fig. 1 (note the different energy and distance scales). In Fig. 2, we can follow the evolution of the 6*s* electron density from the free ion (plot a) to the cluster *in vacuo* at long (plot b) and short (plot c) Yb–Br distances, and to the embedded cluster (plot d).

The ground state of the $(YbBr_6)^{4-}$ cluster *in vacuo* shows a very shallow minimum at a very long Yb–Br distance, 3.59 Å, which indicates the weak binding ability of Yb(II) *in vacuo*. The more diffuse electron density of the 6*s* atomic orbital can be retained within the Br_6 cage (Fig. 2b) only at long Yb–Br distances and a minimum is observed at 3.75 Å, 0.16 Å away from the ground state minimum. The transition energy, 10800 cm^{-1}, is not far from that of the free ion (cf. Table 1). As the calculations cover lower Yb–Br distances, a sudden change is observed in the $4f^{13}\ 6s^1$–$^3A_{2u}$ excited state energy and wave function around 3.3 Å, which results in a new minimum at 2.93 Å and −1900 cm^{-1} with respect to the $4f^{14}$–$^1A_{1g}$ state. The plot of the 6*s* molecular natural orbital (Fig. 2, c) shows a significant charge spill outside the Br_6 cage, which indicates that Yb can no longer keep the excited electron localized. The binding observed corresponds to the formation of an Yb-trapped exciton[24,25] that consists of a hole in the 4*f* shell and an excited electron, which, although still bound to the Yb atom, shows a significant delocalization beyond the $(YbBr_6)^{4-}$ cluster boundaries. The charge spill results in a decrease of the electron repulsion with the Br_6 cage and the energy drops some 12700 cm^{-1} from the long distance minimum. At the same time, the bond distance becomes very close to that of a trivalent Yb cluster, as it can be observed in the left, lower graph of Fig. 1, where we have plotted the potential energy curve of the $4\ f^{13}$–$^3T_{1u}$ ground state of $(YbBr)3_6^{3-}$ *in vacuo*. This result indicates that the divalent oxidation state of Yb is not stable in hexabromide coordination in gas phase and that the $4f^{13}\ 6s^1$ states could lead to complete ionization in gas phase. In order to confirm this, we enlarged the $(YbBr_6)^{4-}$ cluster basis set used from that described in the previous Section (which includes basis functions of the Yb and Br atoms only) to allow for further delocalization of the wave functions, if needed. We tried two different types of basis set extensions. First, we added one *s*-type and one *p*-type functions arbitrarily taken to be the 3*s* and 3*p* atomic orbitals of the Ca atoms surrounding the cluster in the crystal; these functions have been located at the Ca sites without changing the number of electrons in the cluster nor including the Ca embedding potential. The binding energy of the Yb-trapped exciton increased only 20 cm^{-1} in this case, which indicates that the charge leak does not occur through the bonding directions where the Br ligands are located. Second, we added one *s*-type function arbitrarily taken to be the unoccupied 6*s* atomic orbital of the Cs atoms surrounding the cluster in the crystal; these functions were located at the Cs sites and neither the number of electrons in the cluster was changed nor the Cs embedding potential was used. In this case, the energy of the $4f^{13}\ 6s^1$–$^3A_{2u}$ state (at 2.93 Å) relative to that of the ground state $4f^{14}$–$^1A_{1g}$ (at 3.59 Å) changed from –1900 cm^{-1} (without the new *s*-type function) to –2600 cm^{-1} (with the new *s*-type function). When

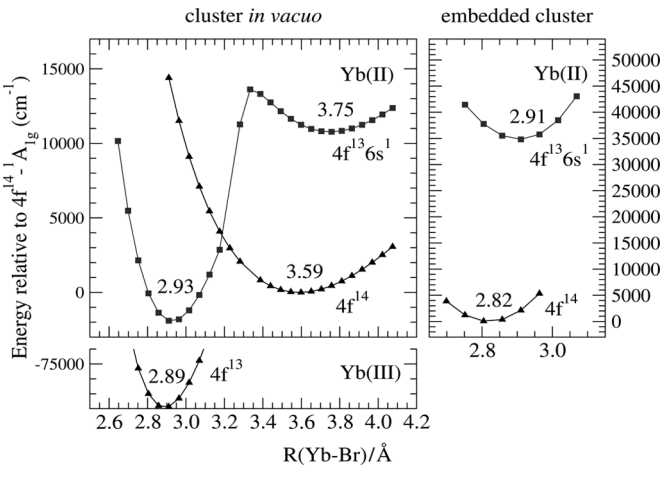

FIGURE 1 **Potential energy curves of the $4f^{14}$–$^1A_{1g}$ and $4f^{13}\ 6s^1$–$^3A_{2u}$ states of the $(YbBr_6)^{4-}$ cluster *in vacuo* (up, left) and embedded in the $CsCaBr_3$ host (right), and of the $4f^{13}$–$^2T_{1u}$ ground state of $(YbBr_6)^{3-}$ *in vacuo* (down, left). All energies have been calculated at the CASSCF level. The $CsCaBr_3$ AIMP embedding potential has been used when indicated. Note the different energy and Yb–Br distance scales in the graph on the right.**

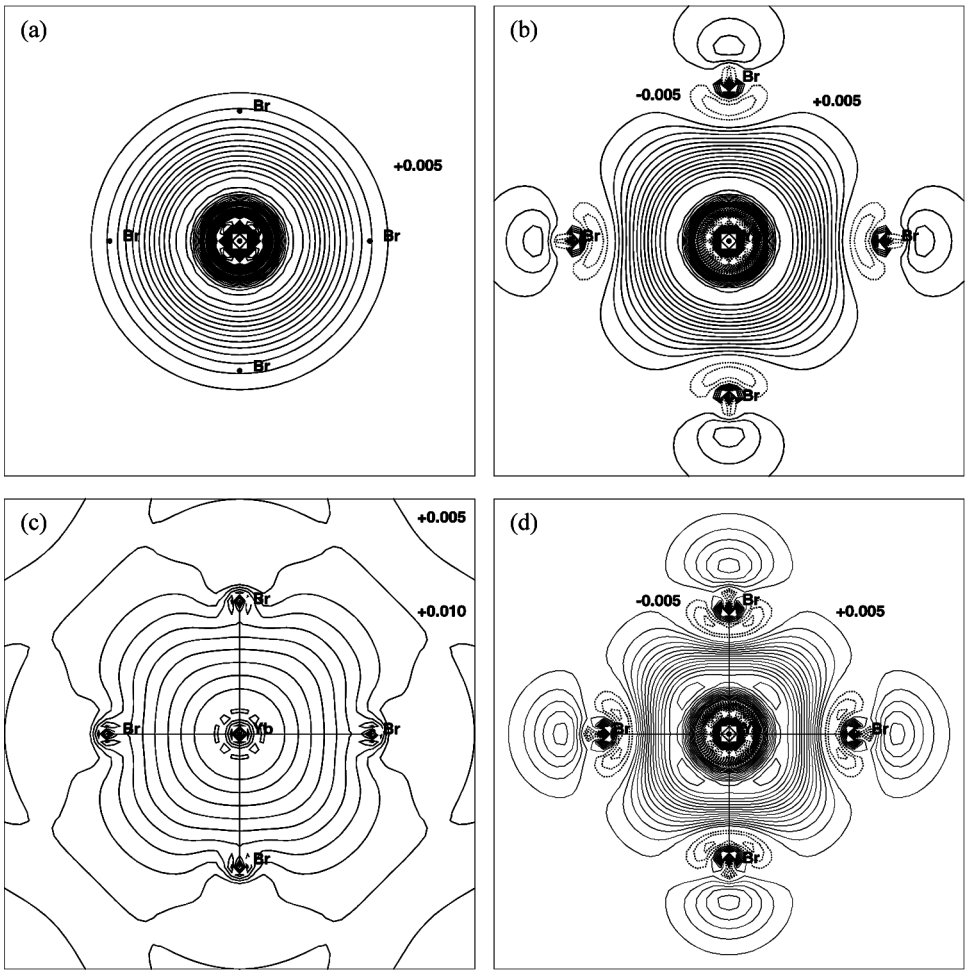

FIGURE 2 **(a): 6*s* atomic natural orbital of the $4f^{13}\ 6s^1$–^3F_u excited state of Yb^{2+} ion in gas phase; Br labels have been plotted at the coordinates where they appear in plot (c). (b): molecular natural orbital of main character 6*s* in the $4f^{13}\ 6s^1$–$^3A_{2u}$ state of the $(YbBr_6)^{4-}$ cluster *in vacuo*, calculated at R(Yb–Br) = 3.75 Å, plotted in the equatorial plane of the $YbBr_6$ octahedron. (c): same as (b), for R(Yb–Br) = 2.93 Å. (d): same as (b), for the $(YbBr_6)^{4-}$ cluster embedded in $CsCaBr_3$ and at R(Yb–Br) = 2.91 Å.**

the Cs 6*s* atomic function was splitted leading to 2 and 6 *s*-type functions, respectively, by realeasing, as usual, the more diffuse Gaussian primitives of the atomic orbital expansion, the energy difference became –23500 and –31700 cm^{-1}, respectively (it should be noted that the basis set effects on the energy of the local $4f^{14}$–$^1A_{1g}$ ground state were negligible). At the same time, the molecular natural orbital of *s*-type became increasingly delocalized and different from a molecular orbital of Yb 6*s* character. This numerical experiment describes the ionization of the $(YbBr_6)^{4-}$ cluster into a $(YbBr_6)^{3-}$ cluster plus a free electron within the framework of a local basis set and shows that the charge leak occurs through the $4f^{13}\ 6s^1$ states and across the (111) directions; the latter illustrates again the repulsive effect of the Br ligands electronic densities.

The charge spill observed in the $4f^{13}\ 6s^1$–$^3A_{2u}$ state, which ultimately leads to ionization, is prevented when the host embedding potentials are used in the $CsCaBr_3$: $(YbBr_6)^{4-}$ embedded cluster calculations and a 6*s* electronic density, basically localized inside the Br_6 cage, is restored (see Fig. 2d). The localization enforced by the embedding increases the electron repulsion within the Br_6 cage and the energy of the $4f^{13}\ 6s^1$ state is strongly risen, this resulting in the large destabilization compared to the free ion value, commented above (see Fig. 1, right).

Although we focus here on the question of why the $4f^{13}\ 6s^1$ states are destabilized in the crystal, these results are connected with a more general matter pertaining to the behavior of $f^{N-1}\ s^1$ states of lanthanide and actinide impurities (in different oxidation

states and halide coordinations in crystals) as localized states or as impurity-trapped excitons. Although more evidences should be accumulated, a simple model of the interactions leading to either type of electronic structure is being envisaged. The model cannot substitute the *ab initio* theoretical methods, but it serves to transmit the essence of their results in simple terms. So, when one $4f$ ($5f$) electron is excited to the much more diffuse $6s$ ($7s$) orbital, which strongly overlaps the electronic density of the ligands cage, strong electron-electron repulsions appear between the $6s$ ($7s$) electron and the ligands that provoke a significant charge spill outside the cluster volume, which allows for considerable bond length shrinkage, all of which leads to the formation of impurity-trapped exciton states.[25] Therefore, the size of the repulsive ligands cage, relative to the extent of the diffuse atomic orbital of the impurity, seems to be a driving force for charge spill (small repulsive cage) and formation of an excitonic state or, on the contrary, for the formation of a very high energy local state (large repulsive cage) whose electron density may still stay within the cluster volume. This explains why in crystals like Cs_2GeF_6:U^{4+} (Ref. 25) the $5f^1$ $7s^1$ excited states are impurity-trapped excitons lying between the $5f^1$ $6d(t_{2g})^1$ and $5f^1$ $6d(e_g)^1$ manifolds, whereas in Cs_2ZrCl_6:U^{4+},[20] Cs_2NaYCl_6:U^{3+} (Ref. 26), and $CsCaBr_3$:Yb^{2+} (as we show here) with larger hexachloride and hexabromide cages, the $5f^17s^1$, $5f^27s^1$, and $4f^{13}$ $6s^1$ excited states appear at higher energies and their electronic structure does not show impurity-trapped exciton characteristics (delocalized electron density and impurity–ligand bond lengths close to the ionized defect). Here, we have analyzed the matter with a new perspective by including the cluster *in vacuo* calculations, which allows to separate the effects of the ligands cage from the effects of the host ions beyond it. We have seen that the $4f^{13}$ $6s^1$ states of $(YbBr_6)^{4-}$ lead to ionization in gas phase and that this charge leak is prevented in the $CsCaBr_3$ solid by the embedding interactions with the host, which, in turn, explains their relatively high energy. Further work on Yb^{2+}-doped crystals in other coordinations and with different ligands ($SrCl_2$ and SrF_2), in progress in our laboratory, should reveal whether the localization enforced by the host embedding leads to well localized high-energy f^{N-1} s^1 states or to not so localized lower lying impurity-trapped excitons. The role of the $4f^{13}$ $6s^1$ states in the absorption spectrum of $CsCaBr_3$:Yb^{2+} crystal has been discussed in detail in Sanchez-Sanz et al.[9]

CONCLUSIONS

Very large embedding effects on the $4f^{13}$ $6s^1$ excited states of Yb^{2+} are found in Yb^{2+}-doped $CsCaBr_3$, which are originated beyond its first coordination shell and increase the $4f^{14} \rightarrow 4f^{13}6s^1$ electronic transitions by some $20000\,cm^{-1}$ with respect to their gas phase values. As a consequence, these states, which are found among the lowest lying states of Yb^{2+} in gas phase, are pushed up in energy to the conduction band of the host. *Ab initio* quantum chemical calculations have been done in the free ion, in the $(YbBr_6)^{4-}$ cluster *in vacuo*, and in the $(YbBr_6)^{4-}$ defect cluster embedded in the $CsCaBr_3$ host to reveal the nature of the strong destabilization, which is not due to dynamic electron correlation nor to spin-orbit effects. The results of the $(YbBr_6)^{4-}$ cluster *in vacuo* reveal that the $4f^{13}6s^1$ states undergo a sudden energy and electron density change at short Br–Yb distances, which results in the formation of an Yb-trapped exciton, which evolves to full ionization of the $(YbBr_6)^{4-}$ cluster as the molecular basis set used is enlarged to allow for delocalization. The charge spill is reversed by the embedding interactions with the host ions located beyond the $YbBr_6$ moiety and localization of the $6s$ electronic density inside the Br_6 cage is restored. The localization enforced by the embedding interactions increases the electron repulsion within the Br_6 cage and the energy of the $4f^{13}$ $6s^1$ states is strongly risen.

ACKNOWLEDGMENTS

This research was supported in part by Ministerio de Ciencia e Innovación, Spain, under contracts CTQ2005–08550 and MAT2008–05379. G.S-S. acknowledges an FPI fellowship from Ministerio de Ciencia e Innovación, Spain.

REFERENCES

1. Bryant, B. W. Spectra of doubly and tryply ionized Ytterbium, Yb III and Yb IV. *J. Opt. Soc. Amer.* **1965**, *55*, 771–775.
2. McClure, D. S.; Kiss, Z. Survey of the spectra of the divalent rare-earth ions in cubic crystals. *J. Chem. Phys.* **1963**, *39*, 3251–3257.
3. Piper, T. S.; Brown, J. P.; McClure, D. S. fd and $f^{13}d$ configurations in a crystal field, and the spectrum of Yb^{++} in cubic crystals. *J. Chem. Phys.* **1967**, *46*, 1353–1358.

4. Rubio, J. Doubly-valent rare-earth ions in halide crystals. *J. Phys. Chem. Solids* **1991**, *52*, 101–174.
5. Pan, Z.; Duan, C.; Tanner, P. A. Electronic spectra and crystal field analysis of Yb^{2+} in $SrCl_2$. *Phys. Rev. B* **2008**, *77*, 085114 1–13.
6. Judd, B. R. Correlation crystal fields for lanthanide ions. *Phys. Rev. Lett.* **1977**, *39*, 242–244.
7. Morrison, C. A. Host dependence of the rare-earth ion energy separation $4f^N$–$4f^{N-1}$nl. *J. Chem. Phys.* **1980**, *72*, 1001–1002.
8. Bettinelli, M.; Moncorgé, R. Correlation between the 5d-level position of Ce(3+) and of the other Ln(3+) ions in solids. *J. Lumin.* **2001**, *92*, 297–289.
9. Sánchez-Sanz, G.; Seijo, L.; Barandiarán, Z. Energy gaps in the $4f^{13}5d^1$ manifold and multiple spontaneous emissions in Yb^{2+}-doped $CsCaBr_3$. *J. J. Phys. Chem. A* **2009**, *113*, 12591–12598.
10. Roos, B. O.; Taylor, P. R.; Siegbahn, P. E. M. A complete active space SCF method (CASSCF) using a density matrix formulated super-CI approach. *Chem. Phys.* **1980**, *48*, 157–173; Siegbahn, P. E. M.; Heiberg, A.; Almlöf, J.; Roos, B. O. The complete active space SCF (CASSCF) method in a Newton-Raphson formulation with application to the HNO molecule. *J. Chem. Phys.* **1981**, *74*, 2384–2396; Siegbahn, P.; Heiberg, A.; Roos, B.; Levy, B. A comparison of the super-CI and the Newton-Raphson scheme in the complete active space SCF method. *Phys. Scr.* **1980**, *21*, 323–327.
11. Andersson, K.; Malmqvist, P.-Å.; Roos, B. O.; Sadlej, A. J.; Wolinski, K. Second-order perturbation theory with CASSCF referente function. *J. Phys. Chem.* **1990**, *94*, 5483–5488.
12. Andersson, K.; Malmqvist, P.-Å.; Roos, B. O. Second order perturbation theory with a complete active space self consistent field reference function. *J. Chem. Phys.* **1992**, *96*, 1218–1226.
13. Zaitsevskii, A.; Malrieu, J. P. Multi-partitioning quasidegenerate perturbation theory. A new approach to multireference Møller-Plesset perturbation theory. *Chem. Phys. Lett.* **1995**, *233*, 597–604.
14. Finley, J.; Malmqvist, P.-Å.; Roos, B. O.; Serrano-Andrés, L. The multi-state CASPT2 method. *Chem. Phys. Lett.* **1998**, *288*, 299–306.
15. Seijo, L.; Barandiarán, Z.; Ordejón, B. Transferability of core potentials to f and d states of lanthanide and actinide ions. *Mol. Phys.* **2003**, *101*, 73–80.
16. Barandiarán, Z.; Seijo, L. The ab initio model potential method. Cowan–Griffin relativistic core potentials and valence basis sets from Li (Z = 3) to La (Z = 57). *Can. J. Chem.* **1992**, *70*, 409–415.
17. Karlström, G.; Lindh, R.; Malmqvist, P. A.; Roos, B. O.; Ryde, U.; Veryazov, V.; Widmark, P. O.; Cossi, M.; Schimmelpfennig, B.; Neogrady, P.; Seijo, L. MOLCAS: A program package for computational chemistry. *Comput. Mater. Sci.* **2003**, *28*, 222–239.
18. Seijo, L. Relativistic ab initio model potential calculations including spin-orbit effects through the Wood-Boring Hamiltonian. *J. Chem. Phys.* **1995**, *102*, 8078–8088.
19. Seijo, L.; Barandiarán, Z. The ab initio model potential method: A common strategy for effective core potential and embedded cluster calculations. In *Computational Chemistry: Reviews of Current Trends*; Leszczyński, J., Ed.; World Scientific: Singapore, 1999, p. 55–152.
20. Barandiarán, Z.; Seijo, L. Structure and spectroscopy of U^{4+} defects in Cs_2ZrCl_6. Ab initio theoretical studies on the $5f^2$ and $5f^16d^1$ manifolds. *J. Chem. Phys.* **2003**, *118*, 7439–7456.
21. Llusar, R.; Casarrubios, M.; Barandiarán, Z.; Seijo, L. Ab initio model potential calculations on the electronic spectrum of Ni(2+)-doped MgO including correlation, spin-orbit and embedding effects. *J. Chem. Phys.* **1996**, *105*, 5321–5330.
22. Vallet, V.; Maron, L.; Teichteil, C.; Flament, J.-P. A two-step unconnected determinantal effective Hamiltonian-based SO-CI method. *J. Chem. Phys.* **2000**, *113*, 1391–1402.
23. Detailed core and embedding AIMP data libraries in electronic format are available from the authors upon request or directly at the address http://www.uam.es/quimica/aimp/Data/AIMPLibs.html. See also Karlström et al.[17]
24. McClure, D. S.; Pédrini, C. Excitons trapped at impurity centers in highly ionic crystals. *Phys. Rev. B* **1985**, *32*, 8465–8468.
25. Ordejón, B.; Seijo, L.; Barandiarán, Z. Geometry and electronic structure of impurity-trapped excitons in Cs_2GeF_6:U^{4+} crystals. The $5f^17s^1$ manifold. *J. Chem. Phys.* **2007**, *126*, 194712 1–8.
26. Ruipérez, F. Estudios teóricos ab initio de impurezas en cristales iónicos: Estructura y espectroscopía de U^{3+} y otros iones de elementos f en las configuraciones f^N, $f^{N-1}d^1$ y $f^{N-1}s^1$ en Cs2NaYCl$_6$, Ph. D. Thesis Dissertation, Universidad Autónoma de Madrid, 2007.